

# Thermal/Electronic Transport Properties and Two-Phase Mixtures in $\text{La}_{5/8-x}\text{Pr}_x\text{Ca}_{3/8}\text{MnO}_3$

K. H. Kim<sup>1,\*</sup>, M. Uehara<sup>1,†</sup>, C. Hess<sup>1,‡</sup>, P. A. Sharma<sup>1</sup> and S-W. Cheong<sup>1,2</sup>

<sup>1</sup>*Department of Physics and Astronomy, Rutgers University, Piscataway, New Jersey 08854*

<sup>2</sup>*Bell Laboratories, Lucent Technologies, Murray Hill, New Jersey 07974*

(to appear in Phys. Rev. Lett.)

We measured thermal conductivity  $\kappa$ , thermoelectric power  $S$ , and dc electric conductivity  $\sigma$  of  $\text{La}_{5/8-x}\text{Pr}_x\text{Ca}_{3/8}\text{MnO}_3$ , showing an intricate interplay between metallic ferromagnetism (FM) and charge ordering (CO) instability. The change of  $\kappa$ ,  $S$  and  $\sigma$  with temperature ( $T$ ) and  $x$  agrees well with the effective medium theories for binary metal-insulator mixtures. This agreement clearly demonstrates that with the variation of  $T$  as well as  $x$ , the relative volumes of FM and CO phases drastically change and percolative metal-insulator transition occurs in the mixture of FM and CO domains.

PACS numbers: 75.30.Vn, 72.20.Pa, 72.15.Eb, 72.80.Tm

Immense resurgent activities on mixed-valent manganites reveal the importance of Jahn-Teller-type electron/lattice coupling in addition to the double exchange mechanism [1–4]. Another important aspect of manganites is the existence of various-scale, real-space variation of physical properties or parameters. For example, even though the orthorhombicity of the average structure drastically decreases with the replacement of La by divalent ions in  $\text{LaMnO}_3$ , the large variation of local Mn-O bond lengths still remains intact [5]. In high divalent-ion doping ranges, charge ordering results in sheet-like arrangements of  $\text{Mn}^{3+}$  and  $\text{Mn}^{4+}$  ions with 10-30 Å length-scales [6]. Furthermore, ferromagnetic resonance experiments have shown the presence of two types of signals in ferromagnetic manganites, which was interpreted as evidence of electronic phase separation [7]. Various experiments suggest the existence of magnetic polarons or mobile ferromagnetic clusters at high temperature ( $T$ ), which could be viewed as resulting from dynamic phase separation [8,9]. Recently, an electron diffraction study on low Curie temperature ( $T_C$ ) manganites has revealed that there coexist ferromagnetic (FM)-metallic and CE-type charge-ordered (CO), insulating domains [10,11]. It has been emphasized that this particular type of static phase separation is responsible for colossal magnetoresistance in low  $T_C$  manganites. Various theoretical models for mixed-valent manganites also reveal the general tendency of static or dynamic electronic phase separation [12].

The transport properties of metal-insulator (M-I) mixtures have been perennial topics for both theoretical and experimental condensed matter physics [13]. Most of the experiments were performed on films with deposited M-I mixture [14] or artificial bulk M-I composites prepared under pressure [15]. The total electric and thermal conductivity and thermoelectric power of binary M-I mixtures were successfully explained by the effective medium theories [13–18].

In this letter, we report the absolute values of

the magnetization  $M$ , thermal conductivity  $\kappa$ , thermoelectric power  $S$ , and dc electric conductivity  $\sigma$  of  $\text{La}_{5/8-x}\text{Pr}_x\text{Ca}_{3/8}\text{MnO}_3$  with various  $x$  and  $T$ . Various aspects of our results are consistent with the coexistence of FM and CO phases, whose relative volumes change with both  $T$  and  $x$ , and the percolative M-I transition in FM-CO mixtures. Furthermore, the  $T$  and  $x$  dependence of  $\sigma$ ,  $\kappa$ , and  $S$  agrees well with the (general) effective medium theories for M-I mixtures.

High-quality polycrystalline specimens of  $\text{La}_{5/8-x}\text{Pr}_x\text{Ca}_{3/8}\text{MnO}_3$  with  $x=0.0, 0.1, 0.2, 0.25, 0.3, 0.35, 0.375, 0.40, 0.42, \text{ and } 0.625$  have been prepared with the standard solid state reaction. We fixed the Ca concentration at 3/8 because our previous studies showed that  $T_C$  is optimized at this particular Ca doping level [6].  $\sigma$  of all specimens with accurate geometry was measured with the standard four probe method, and  $M$  was measured with a SQUID magnetometer. Both  $\kappa$  and  $S$  of the representative samples ( $x=0.0, 0.1, 0.25, 0.35, 0.375, 0.42, \text{ and } 0.625$ ) have been measured from 8 to 310 K with the steady state method. A radiation shield was used to obtain absolute  $\kappa$  values [19].

The systematic  $T$ -dependent and  $M/H$  curves are shown in Fig. 1.  $M/H$  curves were measured in  $H = 2$  kOe, which was carefully chosen to align FM domains without influencing the CO insulating phase. These results indicate that  $\text{La}_{5/8-x}\text{Pr}_x\text{Ca}_{3/8}\text{MnO}_3$  ( $x=0.0$ ) is, basically, FM-metallic below 275 K, and that the ground state of  $\text{Pr}_{5/8}\text{Ca}_{3/8}\text{MnO}_3$  ( $x=0.625$ ) is CO-insulating below 225 K. The behaviors of  $\sigma$  and  $M/H$  for other  $x$  compositions are systematically in-between those for  $x=0.0$  and 0.625. Open circles (Fig. 1 (a)) represent the M-I transition points where  $\sigma$  becomes (local) minimum [20]. Open circles in Fig. 1 (b) show the  $M/H$  values at the M-I transition points determined from the curves. The average of those  $M/H$  values (dotted line) is  $17 \pm 2$  % of 8.1 emu/mol, the saturated  $M/H$  value of  $x=0.0$ . Thus, with changing  $T$ , the M-I transition occurs when  $M$  of each sample becomes about 17 % of that of  $x=0.0$ ,

independent from  $x$  value. If we assume that the  $T$ -dependent volume fraction  $f(T)$  of the FM domain is proportional to  $M(T)$  in  $H=2$  kOe, the M-I transition with changing  $T$  occurs when  $f$  reaches  $\sim 0.17$ , close to the three-dimensional percolation threshold ( $f_c$ ). This behavior can be also seen in the variation of  $\sigma$  with  $x$  for fixed  $T$ . In Fig. 2 (a),  $\sigma$  vs.  $M_x(T)/M_{0,0}(T)$  plot is shown at 10 and 100 K for various  $x$ . Interestingly, the samples with  $M_x(T)/M_{0,0}(T) < 0.15$  are in the insulating regions of the curves in Fig. 1, while those with  $M_x(T)/M_{0,0}(T) > 0.17$  are in the metallic regimes. Therefore, with variation of  $x$ , the M-I transition occurs when  $M_x/M_{0,0} \approx 0.15-0.17$ . These observation clearly suggest that the M-I transition with both  $T$  and  $x$  takes place when  $f(T,x) (\equiv M_x(T)/M_{0,0}(T))$  becomes close to  $f_c$ . It is important to note that  $M_{0,0}(T)$  contains the natural  $T$ -dependence of ferromagnetic moment so that  $f(T,x)$  equals to  $M_x(T)/M_{0,0}(T)$  (not  $M_x(T)/M_{0,0}(T=0)$ ).

To gain further insights into the nature of the M-I transition, we measured  $T$ -dependent  $\kappa$  and  $S$  as shown in Fig. 3. First, we note that the estimated  $\kappa_e$  from  $\sigma$ , using the Wiedemann-Franz law, is by two orders of magnitude smaller than the measured  $\kappa(T)$  for all  $x$ , indicating the dominant phonon contribution. Furthermore, at high  $T$  above  $T_C$  or  $T_{CO}$ ,  $\kappa$  always increases when  $T$  is raised, and the magnitude of  $\kappa$  is in the range of 0.5-2 W/mK, comparable to that of amorphous solids [21]. This behavior has been attributed to local anharmonic lattice distortions associated with small polarons [22]. Related to this,  $S(T)$  of all the samples at high  $T$  follows the form  $S_0 + E_g/k_B T$  with the gap energy  $E_g$  systematically increasing from 4 meV ( $x=0.0$ ) to 12 meV ( $x=0.625$ ). These  $E_g$  values are significantly smaller than the activation energies (125 meV:  $x=0.0$  to 175 meV:  $x=0.625$ ) associated with  $\sigma(T)$ . This difference can result from the small polaronic transport [23].

As shown in Fig. 3 (a), with increasing  $x$ ,  $\kappa(T)$  smoothly evolves from that of  $x=0.0$  to that of  $x=0.625$ , and the  $\kappa$  increase at  $T_C$  becomes smaller. Consistently,  $\kappa$  vs.  $M_x(T)/M_{0,0}(T)$  at 10 and 100 K (Fig. 2 (b)) shows that  $\kappa$  varies monotonically from the maximum ( $\kappa$  of  $x=0.0$ ) to the minimum ( $\kappa$  of  $x=0.625$ ). For  $x=0.0$ ,  $\kappa$  at  $T_C$  increases suddenly, probably due to the suppression of local lattice distortions associated with small polarons. For  $x=0.625$ ,  $\kappa(T)$  behaves as in amorphous solids in the entire  $T$  range, except for a slight increase at  $T_{CO}$ .

In comparison with  $\kappa$  and  $\sigma$ ,  $S$  exhibits seemingly different behaviors with  $x$ .  $S$  is very close to the metallic value,  $S$  of  $x=0.0$ , even near  $f_c$  where  $\sigma$  (or  $\kappa$ ) is still significantly smaller than  $\sigma$  (or  $\kappa$ ) of  $x=0.0$ .  $S$  vs.  $M_x/M_{0,0}$  at 100 K (Fig. 2 (c)) clearly demonstrates this tendency;  $S$  is close to zero (slightly negative), and is insensitive to  $M_x/M_{0,0}$  as long as  $M_x/M_{0,0} \sim 10$  %. In contrast,  $\sigma$  for  $M_x/M_{0,0} = 10$  % at 100 K is more than three orders of magnitude smaller than that of  $x=0.0$ . In fact,

$T$ -dependence of  $S$  near  $T_C$  is also consistent with this metallic  $S$  behavior near  $f_c$ . With decreasing  $T$  near  $T_C$ ,  $S$  starts to decrease, i. e., becomes metallic at  $T$  higher than those for  $\kappa$  and  $\sigma$  changes. For example, in the heating curves of  $x=0.35$ ,  $S$  starts to decrease around 130 K, significantly higher than  $T$  (100 K) for abrupt  $\kappa$  increase or  $T$  ( $\sim 110$  K) for  $\sigma$  minimum.

When thermal/electronic transport properties of our systems are viewed as those of M-I mixtures, the above peculiar  $S$  behavior is, in fact, consistent with the theoretical prediction of effective thermoelectric power  $S_E$  by Bergmann and Levy [18]. For an isotropic binary mixture, they showed that in terms of  $\sigma$ ,  $\kappa$ , and  $S$  of each component,  $S_E$  is given by

$$S_E = S_M + (S_I - S_M) \left( \frac{\kappa_E/\kappa_M}{\sigma_E/\sigma_M} - 1 \right) / \left( \frac{\kappa_I/\kappa_M}{\sigma_I/\sigma_M} - 1 \right), \quad (1)$$

where the subscripts M and I refer to metallic and insulating components, respectively.  $\kappa_E$  and  $\sigma_E$  refer to effective thermal and electric conductivity, respectively, of the binary mixture. This equation has been successfully applied to explain  $S$  behaviors of binary Al-Ge films [14]. When  $\sigma_I/\sigma_M \ll \kappa_I/\kappa_M < 1$  (which applies to our system) and for  $f = f_c$ , the above equation leads to  $S_E \approx S_M$ , which explains our experimental results noted above.

To quantitatively compare our results with Eq. (1), we calculated  $S_E$  at every  $T$  [24]. In this comparison, experimental  $\sigma$  and  $\kappa$ , shown in Figs. 1 and 3, were used for  $\sigma_E$  and  $\kappa_E$ , and  $(\sigma_I, \kappa_I, \text{ and } S_I)$  and  $(\sigma_M, \kappa_M, \text{ and } S_M)$  are assumed to be identical with those of  $x=0.0$  and 0.625, respectively. (For large  $x$ , it was difficult to measure  $S$  at low  $T$  due to high resistivity, so we assumed that  $S_I$  changes as  $1/T$ , and that  $\sigma_I$  does exponentially.) The solid lines in Fig. 3 (b) depict the calculated  $S_E$ , using Eq. (1), for heating curves of  $x=0.25$ , 0.35, and 0.42. The calculated curves match with our experimental  $S$  surprisingly well at all  $T$  below  $T_C$  or  $T_{CO}$ .

For  $\sigma_E$  (or  $\kappa_E$ ) of a binary M-I mixture, Mclachlan [16] proposed the general effective medium (GEM) equation,

$$(1-f) \left( \frac{\sigma_I^{1/t} - \sigma_E^{1/t}}{\sigma_I^{1/t} + A\sigma_E^{1/t}} \right) + f \left( \frac{\sigma_M^{1/t} - \sigma_E^{1/t}}{\sigma_M^{1/t} + A\sigma_E^{1/t}} \right) = 0, \quad (2)$$

where  $A=(1-f_c)/f_c$ . The same equation also works for  $\kappa$ . The critical exponent  $t$  is close to 2 in three dimension. This equation has been successfully applied to isotropic inhomogeneous media in wide  $f$  regions including percolation regime [14,16,17].

To apply the GEM equation to  $\sigma(T)$ , we assumed that  $f(T,x) = M_x(T)/M_{0,0}(T)$ ,  $\sigma_M(T) = \sigma(T)$  of  $x=0.0$ , and  $\sigma_I(T) = \sigma(T)$  of  $x=0.625$ . With the parameters  $t=2$  &  $f_c=0.17$ , the calculated  $\sigma_E$  for various  $x$  are shown as solid lines in Fig. 4. At  $T > \sim 80$  K,  $\sigma_E(T)$  nicely matches the experimental  $\sigma(T)$  even if  $\sigma$  changes by 6 orders of

magnitude with  $T$  and  $x$ . However, this agreement does not hold at very low  $T$ . The calculated  $\sigma_E(T)$  at  $T < 80$  K with the same parameters  $t=2$  &  $f_c=0.17$  significantly deviated from the experimental  $\sigma(T)$ . We found that at  $T < 80$  K, the calculated  $\sigma_E(T)$  matches the experimental  $\sigma(T)$  better when  $t$  is increased to  $\sim 4$ . This is more evident in the  $x$  dependence of  $\sigma$  at 10 and 100 K, as shown in Fig. 2 (a).  $\sigma_E(100$  K), calculated with  $t=2$  &  $f_c=0.17$  (solid line), matches the experimental values (open circles) better than that with  $t=4$  &  $f_c=0.17$  (dotted line). However,  $\sigma_E(10$  K), calculated with  $t=4$  &  $f_c=0.15$  (solid line), is closer to the experimental  $\sigma$  (solid circles) than that with  $t=2$  &  $f_c=0.15$  (dashed line) [25]. (The change of  $f_c$  in the range of 0.15-0.17 makes little difference.) These observations demonstrate that  $t$ , normally close to the three dimensional exponent of 2, becomes  $\sim 4$  at very low  $T$ . A similar, drastic increase of  $t$  has been noted in the case of tunneling transport for M-I mixtures [14,26], suggesting that the tunneling process between FM domains is important for  $\sigma$  of our system at very low  $T$  [27].

By using the GEM equation for  $\kappa_E$ , the  $\kappa(T)$  for various  $x$  can be calculated with the assumption that  $\kappa_I(T)=\kappa(T)$  of  $x=0.625$ ,  $\kappa_M(T)=\kappa(T)$  of  $x=0.0$ ,  $t=2$ , and  $f_c=0.17$ . The solid lines in Fig. 3 (a) represent the estimated  $\kappa_E$  for  $x=0.1, 0.25, 0.35$ , and  $0.42$ . In addition, the calculated  $\kappa_E$  as a function of  $M_x/M_{0.0}$  at 10 and 100 K is depicted as solid lines in Fig. 2 (b). Estimated  $\kappa_E$  lines in Figs. 2 and 3 coincide with the experimental data well [28]. In order to confirm self-consistency,  $S_E$  at 10 and 100 K is evaluated by using the calculated  $\sigma_E$  and  $\kappa_E$  (solid lines of Fig. 2 (a) and (b)), and the Eq. (1). The calculated  $S_E$  (solid lines of Fig. 2 (c)) with the variation of  $x$  is in good agreement with the experimental values.

The unambiguous agreement between the measured thermal/electronic transport properties and the calculated values based on Eqs. (1) and (2) strongly indicates that: (1) transport properties are dominated by thermal/electrical conduction in M-I mixtures, (2) the relative volume of the (FM) metallic phase is proportional to the measured  $M(T,x)$ , and (3) the  $T$ -dependent transport and magnetic properties of metallic and insulating phases are always that of  $x=0$  and  $5/8$ , respectively. Combined with the earlier electron diffraction results [10], this successful agreement demonstrates that all of the thermal, electronic, and magneto-transport properties of  $\text{La}_{5/8-x}\text{Pr}_x\text{Ca}_{3/8}\text{MnO}_3$  are dominated by the percolative conduction through FM-metallic domains which is statically mixed with CO insulating domains. One surprising indication from our results is that at least in low  $T_C$  materials ( $x > 0.25$ ), the so-called Curie transition is, in fact, the M-I transition across percolation threshold, and the ordered FM moment changes smoothly near the percolative phase transition  $T$ .

We greatly thank A. J. Millis, G. Kotliar, E. Abraham, and T. W. Noh for useful discussions. We are

partially supported by the NSF-DMR-9802513. K. H. Kim and M. U. are partially supported by the KOSEF and by the JPSJ Fellowship, respectively.

- 
- \* Also at Research Institute of Basic Sciences, Seoul National University, Seoul 151-742, Korea.
  - † Also at Department of Physics, Aoyama-Gakuin University, Tokyo 157-8572, Japan.
  - ‡ Present address: II. Physikalisches Institut, Universität zu Köln, Köln 50937, Germany.
- [1] C. Zener, Phys. Rev. **82**, 403 (1951); P. W. Anderson and H. Hasegawa, *ibid.* **100**, 675 (1955); P. G. de Gennes, *ibid.* **118**, 141 (1960).
  - [2] A. J. Millis, B. I. Shraiman and R. Müller, Phys. Rev. Lett. **77**, 175 (1996); H. Röder, J. Zang and A. R. Bishop, *ibid.* **76**, 1356 (1996).
  - [3] G-M. Zhao *et al.*, Nature **381**, 676 (1996); K. H. Kim *et al.*, Phys. Rev. Lett. **81**, 4983 (1998), and references therein.
  - [4] Y. Murakami *et al.*, Phys. Rev. Lett. **80**, 1932 (1998); S. Ishihara, M. Yamanaka, and N. Nagaosa, Phys. Rev. B **56**, 686 (1997); K. I. Kugel and D. I. Khomskii, JETP Lett. **15**, 446 (1972).
  - [5] D. Louca *et al.*, Phys. Rev. B **56**, R8475 (1997).
  - [6] S-W. Cheong and C. H. Chen, in Colossal Magnetoresistance, Charge Ordering and Related Properties of Manganese Oxides edited by C. N. R. Rao and B. Raveau (World Scientific, Singapore, 1998).
  - [7] G. Allodi *et al.*, Phys. Rev. B **56**, 6036 (1997).
  - [8] J. B. Goodenough and J.-S. Zhou, Nature **386**, 229 (1997); J.-S. Zhou *et al.*, Phys. Rev. Lett. **79**, 3234 (1997).
  - [9] J. M. De Teresa *et al.*, Nature **386**, 256 (1997); M. R. Ibarra *et al.*, Phys. Rev. B **57**, 7446 (1998).
  - [10] M. Uehara *et al.*, Nature **389**, 560 (1999).
  - [11] In the CE-type CO phase,  $\text{Mn}^{3+}$  and  $\text{Mn}^{4+}$  alternate, and eg orbitals of  $\text{Mn}^{3+}$  order.
  - [12] S. Yunoki, A. Moreo, and E. Dagotto, Phys. Rev. Lett. **81**, 5612 (1998).
  - [13] See, for example, Electrical Transport and Optical Properties of Inhomogeneous Media, edited by J. C. Garland and D. B. Tanner (AIP, New York, 1978).
  - [14] See, for example, G. Hurvits, R. Rosenbaum, and D. S. McLachlan, J. Appl. Phys. **73**, 7441 (1993), and references therein.
  - [15] J. S. Ahn *et al.*, Phys. Rev. B **52**, 15 244 (1995).
  - [16] D. S. McLachlan, J. Phys. C **20**, 865 (1987).
  - [17] N. Dupez, D. S. McLachlan, and I. Sigalas, Solid State Commu. **66**, 869 (1988).
  - [18] D. J. Bergman and O. Levy, J. Appl. Phys. **70**, 6821 (1991).
  - [19] To reduce the complexity due to grain boundaries on the measured  $\kappa$  and  $\sigma$ , we used the same, optimized synthesis conditions for all the samples.
  - [20]  $\sigma(T)$  of  $x=0.3$  and  $0.4$  clearly shows local minima

(slope changes) at the percolation points without showing metallic behavior just below the points. This originates from the drastic  $T$ -dependence of  $\sigma$  of the insulating CO domains, as confirmed by the simulation results of  $x=0.3$  in Fig. 4.

- [21] R. Berman, Thermal Conduction in Solids (Oxford University Press, Oxford, 1976).
- [22] D. W. Visser, A. P. Ramirez, and M. A. Submanian, Phys. Rev. Lett. **78**, 3947 (1997); B. Chen *et al.*, Phys. Rev. B **55**, 15 471 (1997); J. L. Cohn *et al.*, *ibid.* **56**, R8495 (1997).
- [23] B. Chen *et al.*, Phys. Rev. B **53**, 5094 (1996); M. Jaime *et al.*, *ibid.* **54**, 11 914 (1996); M. F. Hundley and J. J. Neumeier, *ibid.* **55**, 11 511 (1997); T. T. M. Palstra *et al.*, *ibid.* **56**, 5104 (1997).
- [24] Previous trials to use effective medium theories in manganites (M. Jaime *et al.*, Phys. Rev. B **60**, 1028 (1999) and G. H. Rao *et al.*, J. Phys: Condens. Matter **8**, 5393 (1996)) have focused on explaining mainly  $T$ -dependence of  $S$  or  $\sigma$  in a narrow  $T$  region of one sample.
- [25] To calculate  $f$  values at 10 K, field-cooled  $M$  values were used. These field-cooled values are consistent with saturated magnetic moments from  $M(H)$  curves.
- [26] I. Balberg, Phys. Rev. Lett. **59**, 1305 (1987).
- [27] H. Y. Hwang and S.-W. Cheong, Chap. 9 in Colossal Magnetoresistance Oxides edited by Y. Tokura (Gordon & Breach, London 1999).
- [28] Since the difference between predicted  $\kappa(T)$  values with  $t=2$  and 4 is relatively small, it was difficult to estimate the correct value of  $t$  for  $\kappa$ .

FIG. 1. (a)  $\sigma(T)$  of  $\text{La}_{5/8-x}\text{Pr}_x\text{Ca}_{3/8}\text{MnO}_3$  for cooling (dotted lines) and heating (solid lines). (b)  $M/H$  curves with zero field cooling. Open circles depict the M-I transition points determined from the data.  $T$ -dependent volume fraction of the FM domains,  $f(T)$ , for each  $x$ , was determined as  $f(T,x) = M_x(T)/M_{0.0}(T)$ .

FIG. 2.  $S$ ,  $\kappa$ , and  $\sigma$  values vs.  $M_x/M_{0.0}$  at 10 and 100 K. The lines depict the theoretical predictions by Eqs. (1) and (2). The solid lines in s show the theoretical results with  $t=4$  &  $f_c=0.15$  at 10 K and  $t=2$  &  $f_c=0.17$  at 100 K. The dotted and dashed lines represent the theoretical results with  $t=2$  &  $f_c=0.15$  at 10 K and with  $t=4$  &  $f_c=0.17$  at 100 K, respectively. For the theoretical predictions (solid lines) of  $\kappa$  at 10 and 100 K,  $t=2$  &  $f_c=0.17$  were used.

FIG. 3. (a)  $\kappa(T)$  for cooling (crosses) and heating (solid circles). The solid lines show the predictions of  $\kappa(T)$  (heating) by Eq. (2) with  $t=2$  &  $f_c=0.17$ . (b)  $S(T)$  of  $\text{La}_{5/8-x}\text{Pr}_x\text{Ca}_{3/8}\text{MnO}_3$ . Crosses represent cooling curves for  $x=0.42$  and 0.35, and the other symbols represent heating data. ( $S$  of  $x=0.1$  is very close to that of  $x=0.0$  and 0.25 below  $T_C$  and omitted for clarity.) The solid lines show the predictions of Eq. (1) for  $x=0.25$ , 0.35, and 0.42 with heating.

FIG. 4. Theoretical predictions (solid lines) of  $\sigma(T)$  by the GEM equation (Eq. (2)) with  $t=2$  &  $f_c=0.17$  above  $\sim 80$  K. Solid squares are the experimental data redrawn from Fig. 1.

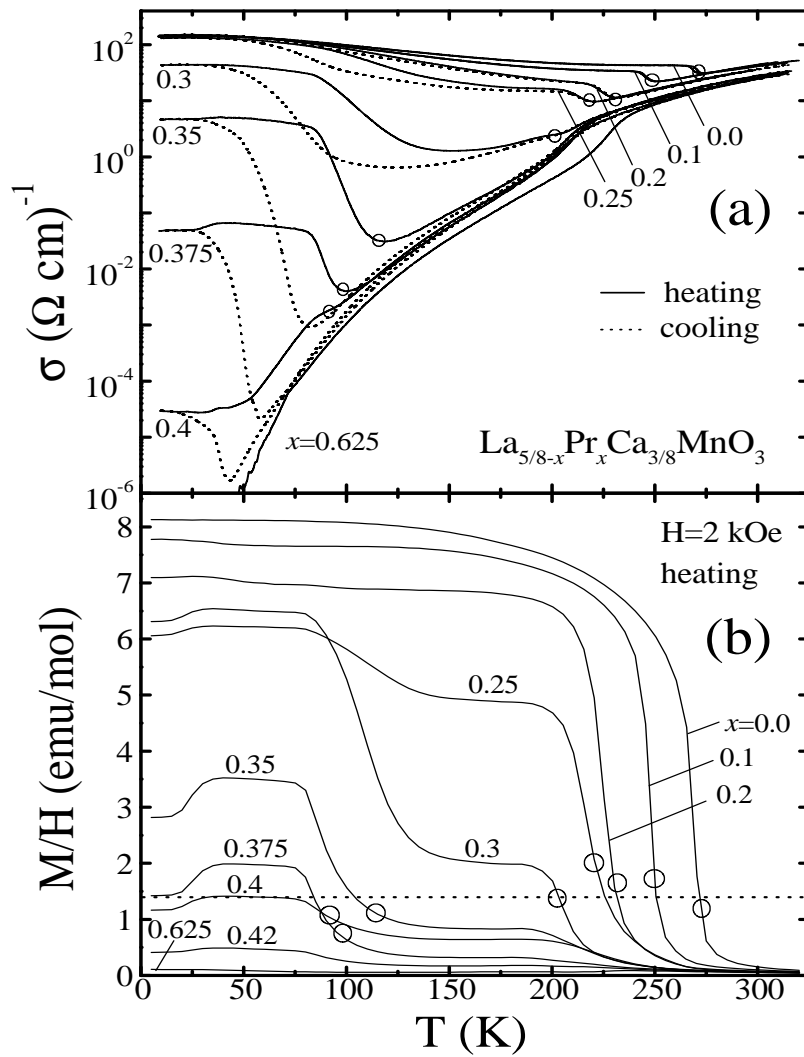


Fig. 1. K. H. Kim *et al.*

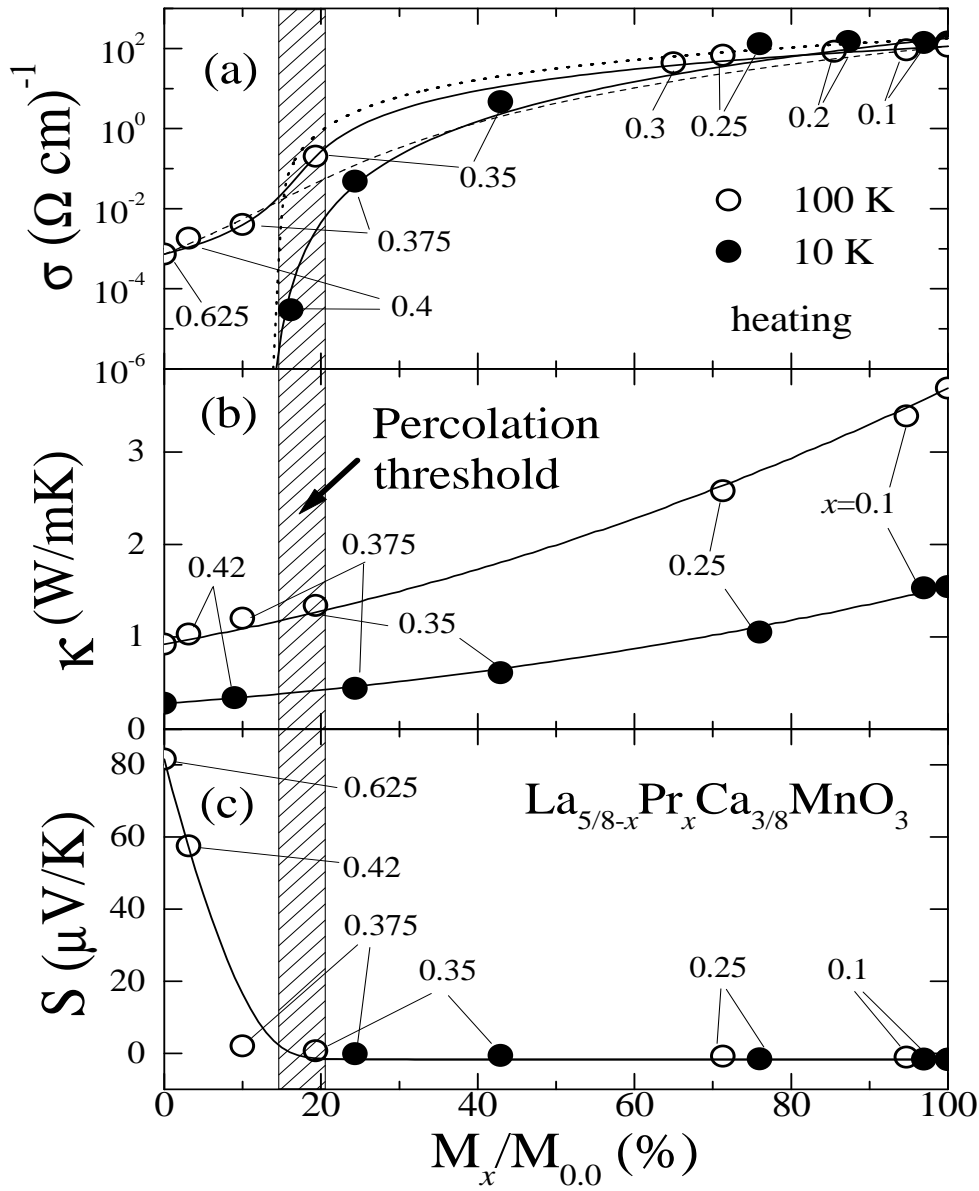


Fig. 2. K. H. Kim *et al.*

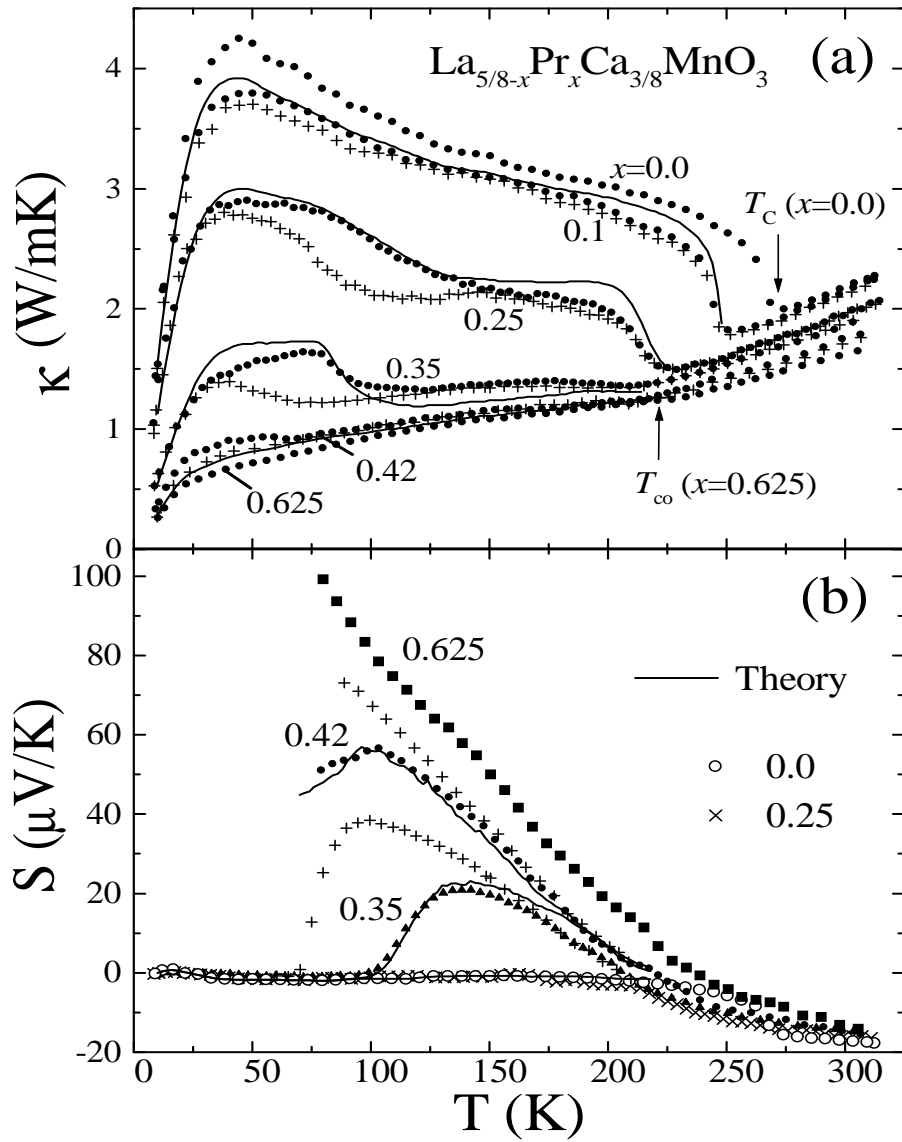


Fig. 3. K. H. Kim *et al.*

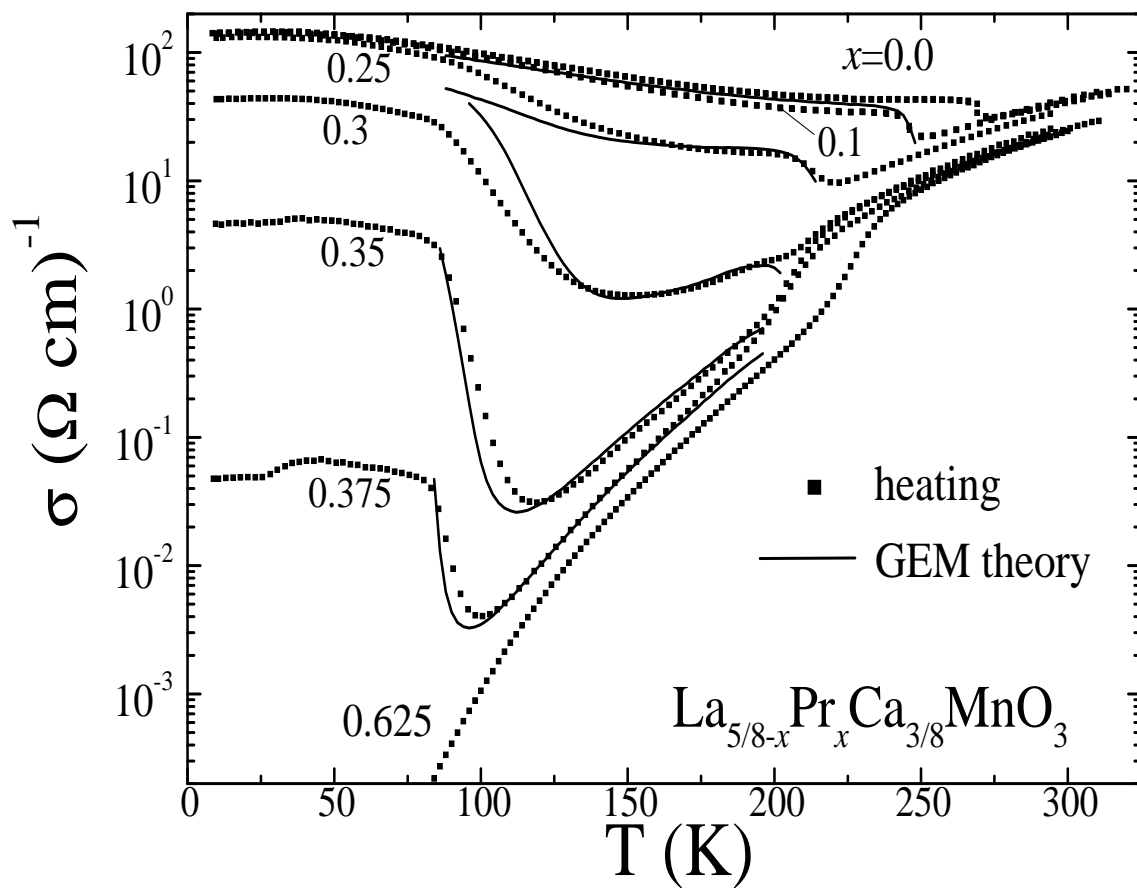


Fig. 4. K. H. Kim *et al.*